scientific reports

Check for updates

OPEN

Exploring the effects of paclitaxel-loaded zein nanoparticles on human ovarian carcinoma cells

Stefania Scicchitano[1,3], Agnese Gagliardi[2,3], Nicola Ambrosio[2], Eleonora Vecchio[1], Cinzia Garofalo[1], Anna Martina Battaglia[1], Francesco Saverio Costanzo[1], Maria Concetta Faniello[1,4]✉ & Donato Cosco[2,4]✉

The development of innovative antitumor formulations that are able to increase the mortality of cancer cells while decreasing the efficacious pharmacological dosage is a fundamental goal of modern oncological research. In this study a paclitaxel (PTX)-nanomedicine was tested on two lines of human high-grade serous ovarian carcinoma (hHGS-OC). Zein, a vegetal protein, was employed to obtain nanoparticles containing the lipophilic compound (NanoPTX) characterized by a mean diameter of 160 nm, a narrow size distribution, a negative zeta potential and a prolonged release of the drug over time. NanoPTX was tested on HEY and COV362 cells demonstrating an increase of apoptosis, particularly on the papillary cystadenocarcinoma cells (55.2% *p* value 0.037 for NanoPTX vs 70.25%, *p* value 0.08 for PTX) with respect to the free form of the drug. The fluorescent nanosystems were characterized by a significant cell uptake after a few hours of incubation and they promoted a reduction in the intracellular reactive oxygen species. The results need to be validated on different hHGS-OC cells and the real efficacy of the proposed nanomedicine needs to be investigated using in vivo models of ovarian carcinoma.

Keywords High grade serous ovarian carcinoma, Nanomedicine, Nanoparticles, Paclitaxel, Zein

Abbreviations

ATCC	American Type Culture Collection
BSC	Biopharmaceutical classification system
DCF	Dichlorofluorescein
DMEM	Dulbecco's Modified Eagle Medium
EOC	Epithelial ovarian cancer
EPR	Enhanced permeability and retention
FACS	Fluorescence-activated cell sorting
FDA	Food and Drug Administration
FT-IR	Fourier-transform infrared spectroscopy
H_2DCFDA	2′-7′-Dichlorodihydrofluoresceindiacetate
hHGS-OC	Human high grade serous-ovarian carcinoma
hOC	Human ovarian carcinoma
MTT assay	3-[4,5-Dimethylthiazol-2-yl]-2,5 diphenyl tetrazolium bromide assay
NanoPTX	Paclitaxel-loaded zein nanoparticles
OC	Ovarian cancer
PBS	Phosphate-buffered saline
PE	Phycoerythrin
PI	Propidium iodide
PTX	Paclitaxel
RB	Rose bengal
ROS	Reactive oxygen species
SDS	Sodium deoxycholate

[1]Laboratory of Biochemistry and Cellular Biology, Department of Experimental and Clinical Medicine, University of Catanzaro Magna Græcia, 88100 Catanzaro, Italy. [2]Department of Health Sciences, University of Catanzaro Magna Græcia, 88100 Catanzaro, Italy. [3]Stefania Scicchitano and Agnese Gagliardi contributed equally to this work. [4]Maria Concetta Faniello and Donato Cosco contributed equally to this work. ✉email: faniello@unicz.it; donatocosco@unicz.it

TEM	Transmission electron microscope
TSA	Total surface area
VNP	Volume of a single nanoparticle

The biopharmaceutical classification system (BSC) categorizes the antineoplastic agent paclitaxel (PTX) as a BCS category IV chemical medication (the most difficult category for oral drug delivery), due to its low systemic bioavailability (less than 8%) and poor pharmacokinetics after administration[1]. Indeed, the bulky chemical structure, the low aqueous solubility (< 0.01 mg/mL) and high lipophilicity (logP 3.96), the recrystallization upon dilution, and the limited permeability in the biological environment are all reasons behind its challenging delivery[2,3].

In order to address these limitations, the first commercially-available form of paclitaxel (Taxol®) was developed as an intravenous infusion formulated by solubilizing the active compound in a co-solvent mixture 1:1 v/v made up of dehydrated ethanol and Cremophor® EL (poly-oxy-ethylated castor oil)[4,5]. However, the organic solvents were responsible for several negative side effects including severe allergic reactions, myelosuppression and neurotoxicity. For this reason, it was necessary to infuse the drug over a longer period and pretreat the patient with steroids and antihistamines[6]. Moreover, PTX exerts its pharmacological activity on both cancerous and normal tissues. Consequently, there is a strong need for innovative formulations able to increase the localization of the drug in the tumor compartments, maximizing its therapeutic efficacy[7,8]. Several polymeric systems have been investigated for the delivery of drugs, but only a few of them have been approved for human use[2,9].

Progress in nanomedicine promotes the development of various nanosystems containing PTX with the aim of improving the therapeutic outcome of the active compound. Most of these are micelles made up of synthetic materials (Genexol PM®, Nanoxel® and Paclical®), while the only liposomal formulation approved for human use (Lipusu®) is available exclusively in Asia. Abraxane® (nab™ paclitaxel), a drug approved by the FDA (Food and Drug Administration) in 2005, is the first albumin-based nanomedicine characterized by nanosystems with a mean diameter of 130 nm. It reaches the tumor through the protein transport pathways, including the gp60 receptor and caveolae-mediated endothelial transcytosis across the blood-tumor barrier[10]. Currently it is being used for the treatment of metastatic breast cancer, locally advanced or metastatic non-small-cell lung cancer and metastatic pancreatic cancer[11].

Proteins are useful biomaterials for the development of nanocarriers of active compounds, due to their biodegradability and their inherent properties[12]. Indeed, protein-based nanosystems can retain a huge variety of drugs, protecting them from degradation and inactivation following their administration, while increasing the amount of active compounds within the tumor mass. This results in a decrease of the unfavorable adverse phenomena on off-target organs. In addition, the high permeability of the tumor vasculature together with the absence of adequate lymphatic drainage promote the preferential accumulation of nanoparticles in the microenvironment of various solid tumors by the enhanced permeability and retention (EPR) effect. Among the various proteins recently employed, zein, a prolamin contained in the endosperm of maize and obtained from the by-products of agricultural processes fulfills all the previously described requirements as well as boasting low cost, bio-adhesion and antioxidant features[13,14]. Indeed, zein nanoparticles, due to their biodegradable and biocompatible nature, can take advantage of the EPR effect to enhance the delivery of active compounds to solid tumors, such as chemotherapeutic drugs.

In view of these findings, PTX has been successfully entrapped within zein nanoparticles, resulting in a novel nanomedicine with high stability and in vitro antitumor efficacy on human cancer cells, such as K562 and MCF-7, with respect to the free form of the drug solubilized in ethanol[15]. In the current study this formulation has been proposed for the first time to improve the treatment of human ovarian cancer (hOC), one of the most lethal gynecological carcinomas, in which PTX is the front-line chemotherapy treatment[16–19].

Results

Physico-chemical characteristics of zein nanoparticles

Recently, the development of zein nanosystems containing PTX (NanoPTX) has been proposed as a suitable formulation able to promote the administration of the active compound in polar media, thus avoiding the main limitations of the organic solvents[15]. Briefly, empty nanosystems stabilized with SD (Nanozein) exhibited a hydrodynamic diameter of approximately 110 nm and a negative Zeta potential of -34 mV. The addition of 0.3 mg/ml of PTX to the protein solution slightly increased the particle size (158 nm) and polydispersity index (0.21), while preserving the suitability of the formulation for parenteral administration (See Table S1). Higher concentrations of PTX caused destabilization, leading to macroaggregates and sedimentation. The Zeta potential remained unchanged (-31 mV) ensuring electrostatic repulsion and preventing aggregation, which guarantees stability for intravenous formulations (See Table S1).

Moreover, the morphological analysis performed using the TEM technique showed that both formulations retained a homogeneous morphology with a well-defined spherical shape, indicating that the addition of PTX did not compromise the colloidal structure, supporting the results of photon correlation spectroscopy (See Fig. 1a,b).

The evaluation of the entrapment efficiency of PTX within zein nanoparticles demonstrated that the active compound is efficiently retained by the polymeric matrix (40%, with respect to the amount of the drug initially added, with a loading capacity of 3.84%)[15] (See Table S1).

The surface properties of zein nanoparticles were also investigated using the Rose Bengal assay (See Fig. 1c). SD-free zein nanoparticles were used as control because the protein is widely recognized as an example of a hydrophobic raw material. The stabilization of nanosystems with SD significantly decreased the hydrophobic characteristics of the colloids.

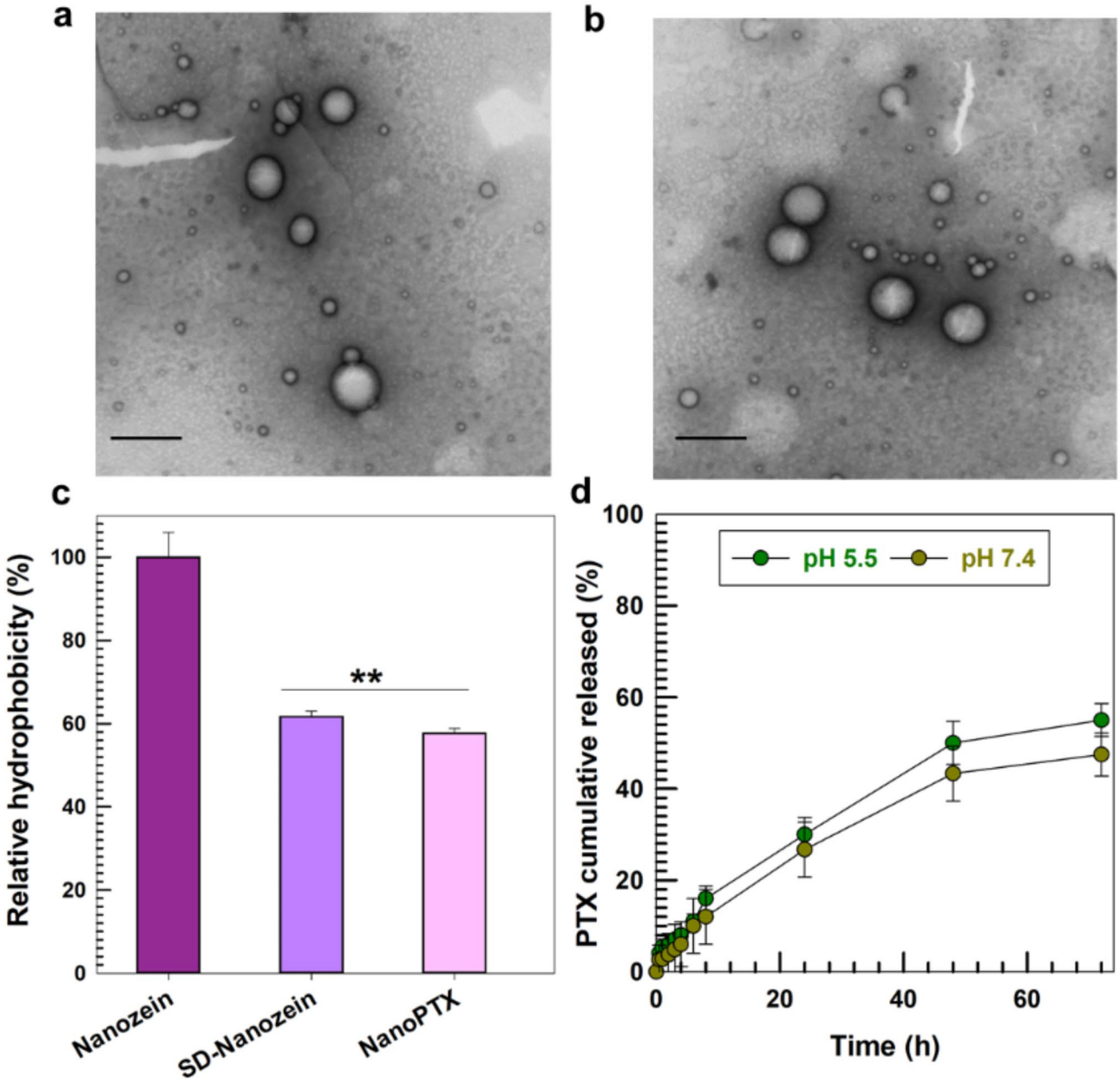

Fig. 1. (**a**) TEM micrographs of Nanozein decorated with SD and (**b**) NanoPTX. Bar = 150 nm. (**c**) Surface hydrophobicity of Nanozein, SD-Nanozein and NanoPTX. $^{**}p < 0.01$ with respect to the surfactant-free zein nanoparticles used as control. (**d**) Release profiles of PTX from zein nanoparticles in physiological (pH 7) and acidic (pH 5) environments as a function of incubation time. The analysis was performed at 37 °C. Values are the mean of three experiments ± standard deviation.

The release profile of PTX from the nanosystems was then investigated in buffers simulating both physiological and tumoral environments. Figure 1 shows that the leakage of PTX from zein nanoparticles was slightly increased in an acidic medium as compared to that obtained in pH 7 (See Fig. 1d).

Various mathematical models were used to analyze the release profile of PTX in order to gain insight into the mechanisms governing the leakage of the drug from the nanocarriers. The correlation coefficient (r) was used as a criterion to select the most consistent theoretical model corresponding to the drug release pattern. According to the obtained r^2, the model that best fits the drug release from the nanosystem was the Higuchi model (0.9825 pH 5.5; 0.9806 pH 7.4), which is typical of polymeric matrix-based systems (Table 1). The results support the conclusion that the primary mechanism involved in the release of the drug is diffusion, as described by Fick's law, exhibiting a square root-time dependence.

Infrared Fourier transform measurements were performed in order to gather information regarding the nature of the interactions occurring between the components of the nanoparticles. Figure 2 shows the FT-IR spectra of the different formulations, their physical mixtures and the compounds employed for the preparation

Release medium	Zero-order	First-order	Higuchi	Korsmeyer-Peppas	Hixson-Crowel
Aqueous solution (pH 5.5)	0.9496	0.9742	0.9825	0.6438	0.9673
PBS (pH 7.4)	0.9472	0.9685	0.9806	0.6533	0.9622

Table 1. Correlation coefficient (r^2) of release kinetics of PTX from zein nanoparticles according to various mathematical models.

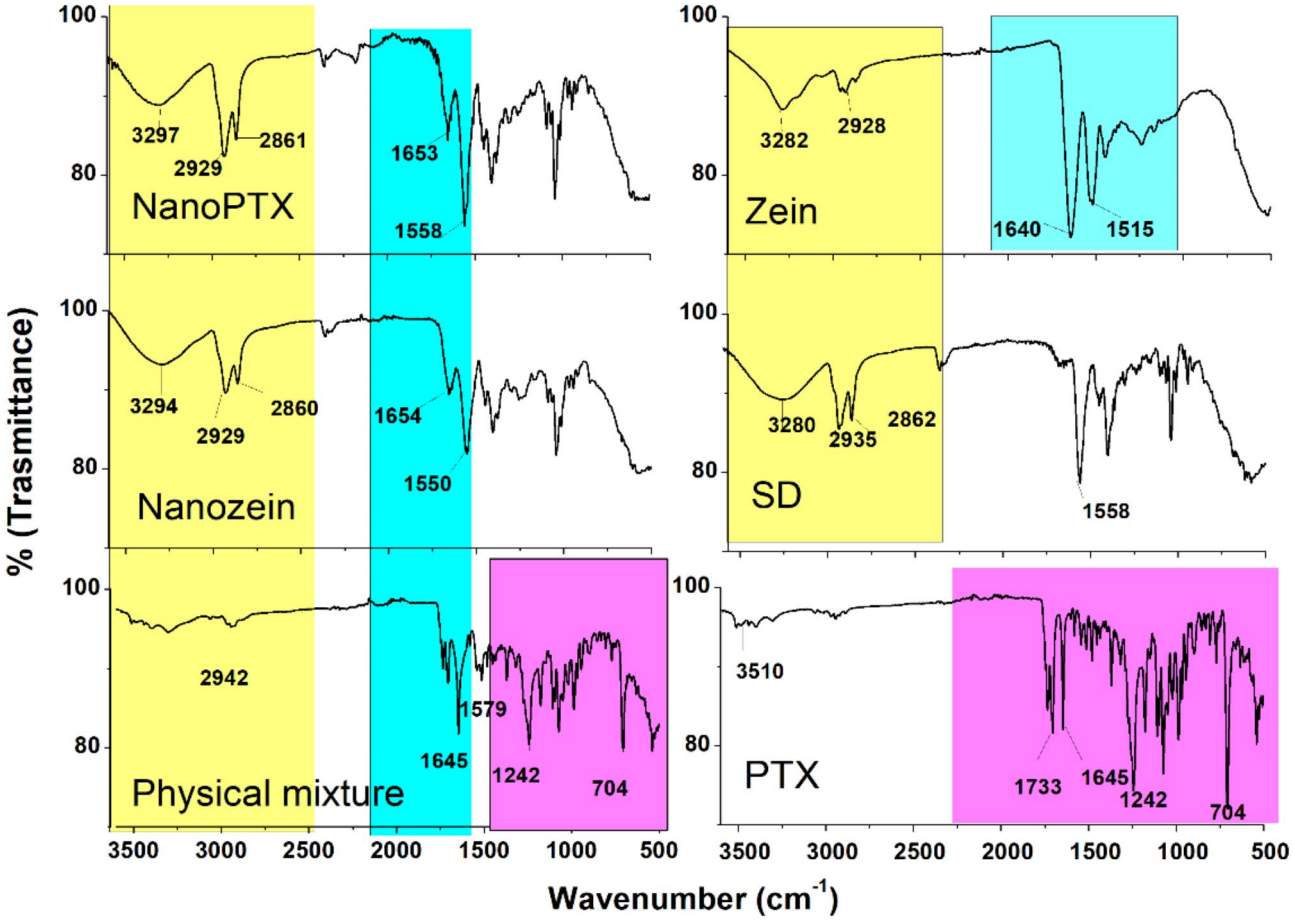

Fig. 2. FT-IR spectra of zein, SD, their physical mixture, empty zein nanoparticles (Nanozein) and PTX-loaded zein nanoparticles (NanoPTX).

of the nanosystems. The spectrum of zein powder showed characteristic absorption bands corresponding to the amide I and amide II groups (at 1640 and 1515 cm^{-1}, respectively). In particular, the C = O stretching vibration was mainly attributed to the amide I group, while the N–H bending coupled to the -C-N stretching vibration was related to the amide II group. In addition, the signal at 3282 cm^{-1} corresponded to an O-H stretching band and the peak related to the asymmetric methyl group (CH_3) was recorded at 2928 cm^{-1} [20–22]. The PTX fingerprints were located at 3510 cm^{-1} (O-H stretch), 1733 cm^{-1} (C=O stretch of the ester group), 1648 cm^{-1} (N–H bond), 1242 cm^{-1} (C-N stretch) and 704 cm^{-1} (C–C stretching), which were also shown in the FT-IR spectra of the physical mixture[23–25]. The SD spectrum showed signals at 2935, 2862, and 1558 cm^{-1} related to the CH stretching vibration and the COO^- stretching vibration modes as previously reported[26]. As can be observed in Fig. 2, the infrared spectrum of the physical mixture was the result of the superimposition of the single spectrum of the three components. In the nanoparticles the O-H stretching peak of zein and SD shifted from 3280 cm^{-1} to 3297 cm^{-1}, while the absorption bands of amides I and II of the protein shifted from 1640 to 1653 cm^{-1} and 1515 to 1558 cm^{-1}, respectively. This demonstrated the presence of hydrogen bonds and electrostatic interactions between the components. It was interesting to observe that the characteristic bands of PTX encapsulated within the zein nanoparticles decreased or vanished completely, probably because they were masked by the polymeric structure, confirming that the active compound was effectively entrapped inside the colloidal systems.

Antioxidant effects of zein nanoparticles on human ovarian carcinoma cell lines

The cytotoxicity of Nanozein was evaluated on Hey and COV362 cells after 24 h incubation by means of a PI assay. As shown in Fig. 3A, Nanozein did not induce significant tumor-cell death at the concentrations of nanosystems tested on both cell lines. Subsequently, intracellular ROS levels were quantified by incubating the cells with increasing amounts of Nanozein for 24 h (See Figure S2). The results of the DCF cytofluorimetric assay, shown in Fig. 3B, demonstrate that Nanozein is able to reduce intracellular ROS in both the cell lines tested, at a concentration of 5 µg/ml in the HEY (FC 0.57 *pvalue* 0.02) and of 10 µg/ml in the COV362 (FC 0.87 *pvalue* 0.05) cell lines. The incubation of fluorescent zein nanoparticles with chemo-sensitive and chemo-resistant cells showed that the colloidal systems were efficiently uptaken and localized in the cytoplasm (See Figure S3).

NanoPTX affects apoptosis in hOC cells

The patients who are diagnosed late are referred to as hOC patients and, although they respond well to surgery and first-line chemotherapy treatments, they often relapse into metastases and develop chemo-resistance[17,18]. The two cell lines utilized in this study are in vitro models of both: the chemo-sensitive cells (the HEY cells, derived from peritoneal deposits), and cells that are resistant to chemotherapeutic taxol-treatment (the COV362 cells, derived from pleural effusion)[27]. Based on the results described above (Fig. 3), the two hOC cell lines were treated with NanoPTX or PTX at the drug concentration of 5 µg/ml (HEY) and 10 µg/ml (COV362), amounts of Nanozein able to decrease the intracellular ROS without any variation in cell viability. The results shown in Fig. 4 demonstrate, as expected, that PTX promotes an increase in the death of HEY chemo-sensitive cells. Notably, NanoPTX induces cell death in a more effective way with respect to PTX in HEY cells (live cells: 85.3% untreated, 55.2% *p* value 0.037 NanoPTX vs 70.25%, *p* value 0.08 PTX) (Fig. 4A). Contrarily, in COV362 (Fig. 4B) neither PTX nor NanoPTX were able to affect cell viability (live cells: 79.77% untreated, 76.35% NanoPTX, 75.15% PTX).

The dose-dependent cytotoxicity of Nanozein, NanoPTX and PTX was also evaluated up to 72 h by MTT assay (Figure S4). As expected, the COV362 cells were more resistant to NanoPTX and PTX with respect to the HEY cells even at high concentrations of the drug (9 nM) and longer incubation times (72 h) (cell viability: Nanozein 87%, NanoPTX 74%, PTX 75%). Vice versa, the HEY cells showed reduced metabolic activity after just 24 h incubation when a drug concentration of 3 nM was employed (cell viability: Nanozein 97%, NanoPTX 79%, PTX 82%). This trend was emphasized after 72 h incubation.

Discussion

The absence of symptoms and of an effective screening program, besides high tumor heterogeneity all mean that two thirds of the patients affected by ovarian cancer are diagnosed at an advanced stage of cancer and have a survival rate of 5 years after receiving surgery and chemotherapy. This makes epithelial ovarian cancer (EOC) one of the most lethal gynecological carcinomas[16,17,28,29]. EOC can be divided into four groups: serous (low and high, the most widespread), mucinous, endometrioid and clear cell, which differ based on their histology and their diffusion. Various therapies have been developed in recent years for the treatment of human high grade serous OC (hHGS-OC), but despite this, the first-line chemotherapy is still PTX alone or in combination with carboplatin[18,19]. PTX is also chosen as a second-line therapy in platinum-resistant tumor recurrences[30]. Several studies have found that high concentrations of PTX can revert microtubule detachment from the centrosomes thus provoking fragmentation of the microtubules, while the administration of low doses [nM] of PTX induces apoptosis, via p53 and p21, together with irreversible mitotic arrest[31,32]. For all these reasons, improving and maximizing the potential of paclitaxel is desirable for the clinical treatment of patients affected by HGS OC.

In this context, the use of zein as a natural protein matrix for the delivery of PTX, as well as the simplicity of the procedure used for the preparation of the nanosystems, are undoubtedly pluses for the nanomedicine discussed in this study because they can fulfill the requisites of sustainability and also a plausible scale-up. The results provided in our previous experimental work demonstrated the suitability of SD-stabilized zein nanoparticles as delivery systems of PTX, showing their remarkable physical stability and the preservation of the in vitro cytotoxic properties of the active compound after its encapsulation in the colloidal systems. These findings prompted us to investigate the efficacy of this formulation on two lines of human high grade serous ovarian carcinoma —for the first time to best of our knowledge. As can be observed in Fig. 1 the hydrodynamic diameter of the nanosystems containing PTX was less than 200 nm which is an important aspect for the accumulation of the nanocarriers in several types of solid tumors due to the passive targeting attributed to the EPR effect[33,34]. Moreover, the stabilization of the zein nanosystems with SD conferred several intriguing features that might encourage their exploitation as innovative antitumor nanotherapeutics; chiefly, the negative surface charges of the nanoparticles could contribute to prolonging their half-life[15]. Indeed, the main parameters that modulate the amount of adsorbed blood proteins are related to the surface characteristics of the nanoparticles, such as zeta potential and hydrophilicity/hydrophobicity. In general, it has been reported that positively-charged nanosystems are characterized by a higher rate of non-specific localization and a shorter plasmatic half-life as compared to those with negative or neutral charges[35,36].

Moreover, the rose Bengal test showed that the addition of SD as a surfactant reduced the hydrophobic surface properties of the colloids. This is a clear indication that the surfactant was integrated into the nanoparticles and can modulate the characteristics of their surfaces and in fact we demonstrated that 1.25% of the amount of the surfactant used during the sample preparation efficiently interacted with the protein matrix. However, the inclusion of the active compound did not promote a significant modulation of Zeta potential with respect to the empty formulation. These features had a great impact on the release profiles of the drug from the zein nanoparticles. Indeed, the slow leakage of PTX may be related to the lipophilic character of the compound which is better retained in the zein matrix as compared to water-soluble molecules, data in agreement with several other experimental investigations[37–42]. In particular, the release of PTX from the colloidal systems was slightly

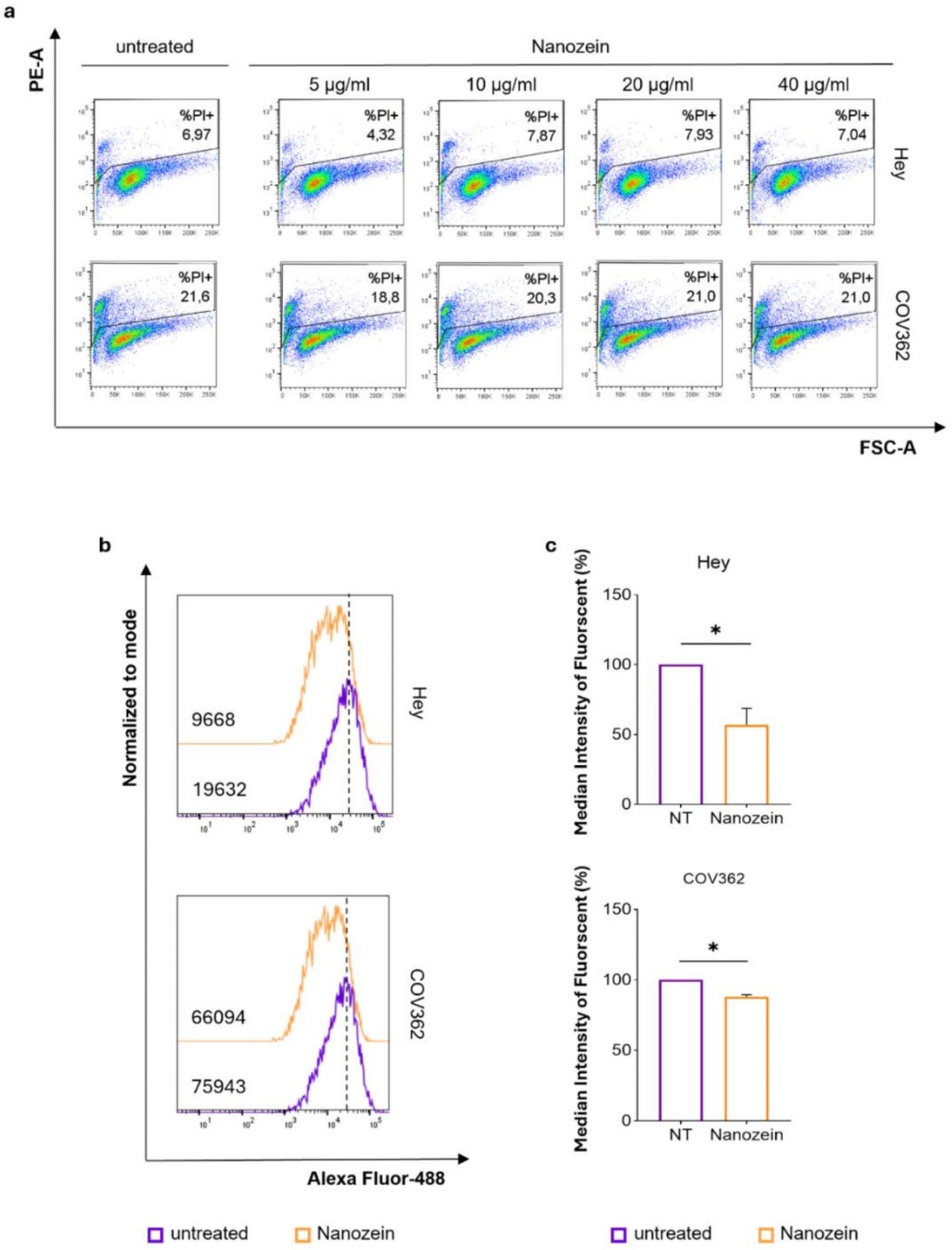

Fig. 3. Nanozein reduces intracellular ROS levels without affecting cell viability. HEY and COV362 cell viability was assessed through propidium iodide (PI) staining following treatments with increasing amounts (5, 10, 20 and 40 µg/ml) of Nanozein for 24 h. The percentage of dead cells (PI positive) are reported in each plot (plots are representative of single experiments) (**a**). CMH_2DCFDA cytofluorimetric assay was carried out. The intracellular ROS levels decreased after incubation with Nanozein for 24 h (HEY and COV362 cells were treated with 5 µg/ml and 10 µg/ml of Nanozein, respectively) (**b**). Histogram values are expressed as mean ± standard deviation of three biological replicates (**c**): $*p < 0.05$, $**p < 0.01$ as compared to non-treated cells. All the experiments were performed in triplicate.

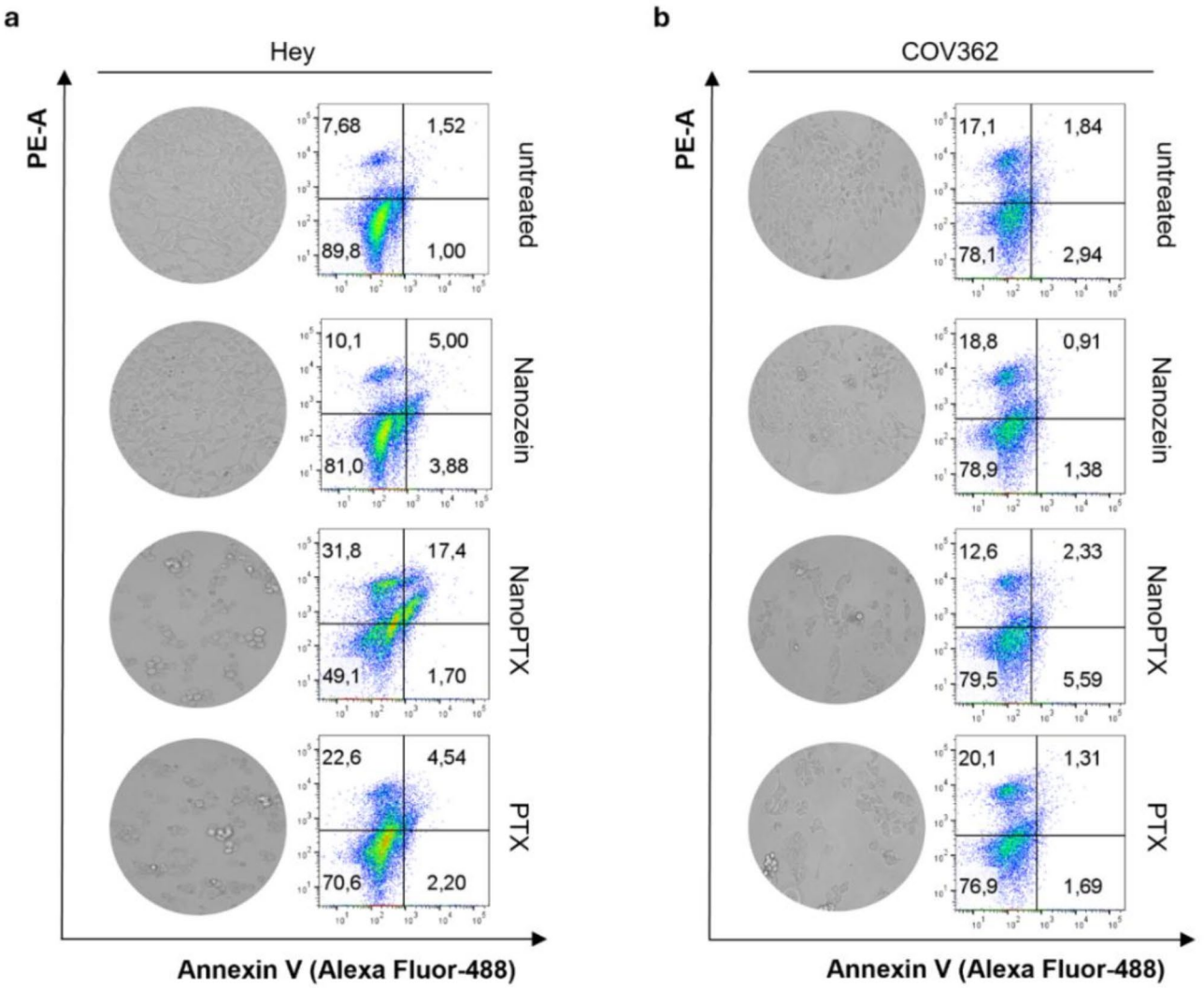

Fig. 4. Representative images and plots of PI/Annexin V-488 apoptosis assays performed on (**a**) HEY and (**b**) COV362 cells. The cells were treated for 24 h with 5 µg/ml (HEY) or 10 µg/ml (COV362) of Nanozein, NanoPTX and PTX. Plots are representative of single experiments. The images of treated and untreated cells were acquired at 20× magnification with Leica LAS X Thunder Imaging Systems (Leica Microsystems Srl, Milan, Italy). All experiments were performed in triplicate.

increased in an acid medium with respect to pH 7.5; this phenomenon was most likely caused by the ability of the protein matrix to swell at low pHs, which allows the PTX to be efficiently released when it reaches the tumor area[13]. However, the formulation was characterized by a constant and prolonged drug release, confirming the peculiar properties of zein nanosystems to retain the active compound for several days, favoring a conceivable localization within the solid tumor compartment and allowing a potential decrease in the number of required administrations and so the related side effects. In addition, the FT-IR analysis confirmed the strong interactions of the PTX with the lipophilic portions of the protein that inhibit the fast release of the active compound. These data agree with several experimental works that demonstrated that zein can strongly interact with terpenoids[43–45].

In order to study the efficacy of zein nanoparticles as a useful drug delivery system, the nanosystems containing PTX (NanoPTX) were used to treat two hHGS OC cell lines and then compared to the same cells treated with free PTX. ROS accumulation induces genomic instability and is a key mechanism for the promotion, initiation and progression of tumor cells[46]. The zein nanoparticles (Nanozein) were observed to accumulate within both chemo-sensitive and chemo-resistant cells (See Figure S2), decreasing the levels of ROS (See Fig. 3). In view of these results, it is conceivable that the antioxidant activity exerted by the nanosystems can affect the metabolism of tumor cells. In addition, NanoPTX significantly enhanced cell death with respect to free PTX (See Fig. 4), providing the rationale of the use of zein nanoparticles as nanocarriers of the lipophilic compound.

In conclusion, the results are encouraging for the conceivable exploitation of the proposed nanomedicine in additional preclinical investigations; namely, the real efficacy of NanoPTX needs to be evaluated on xenograft and orthotropic models of OC and compared to those exerted by the formulations on the market. The pharmacokinetic profile and the biodistribution of the nanomedicine are pivotal parameters that must be

characterized in order to identify the ideal schedule of administration. Last but not least, the opportunity of modulating the surface architecture of the zein nanoparticles through the linkage or deposition of targeting moieties and the co-encapsulation of other active compounds within the protein matrix may be significant technological advancements able to improve the safety and the effectiveness of the formulation for the treatment of OC.

Materials and methods

Zein (CAS number 9010-66-62), sodium deoxycholate monohydrate (SD), paclitaxel (PTX) were all purchased from Merck (Milan, Italy).

Preparation of PTX-loaded zein nanoparticles

The nanoprecipitation method was employed to obtain the zein nanoparticles[15]. In detail, 2 mg/ml of zein were dissolved in 3 ml of an ethanol/water solution (2:1 v/v) at room temperature and added to 5 ml of aqueous phase made up of aqueous solution containing 1.25% w/v of SD, and then mechanically stirred at 600 rpm for 12 h on a magnetic plate to favor the evaporation of the organic solvent[15]. Fluorescent nanoparticles were prepared by solubilizing fluorescein-DHPE (0.1% molar) in the organic phase during sample preparation.

PTX-loaded zein nanosystems (NanoPTX) was prepared by dissolving 0.3 mg/mL of the drug in ethanol. Once the PTX was fully solubilized, an aqueous solution was added, followed by the addition of zein. The organic phase was then mixed with 5 mL of the aqueous phase enriched with 1.25% w/v of SD. The resulting mixture was mechanically stirred at 600 rpm for 12 h on a magnetic plate to facilitate the evaporation of the organic solvent. Successively, the colloidal formulations were ultracentrifuged at 90 k rpm for 60 min at 4 °C, or suitably purified by using Amicon® Ultra centrifugal filters (cut-off 10 kDa). In detail, 1 ml of the nanoparticle suspension was put into the Amicon® filter unit and then centrifuged at 4000 rpm for 20 min. The suspension contained in the filter was collected before the cytotoxicity experiments.

Physico-chemical characterization

The evaluation of the mean sizes, polydispersity index and Zeta potential were performed using photon correlation spectroscopy with a Zetasizer Nano ZS (Malvern Panalytical Ltd., Spectris plc, England) and applying the third order cumulant correlation function as previously reported. The results were expressed as the mean of three different experiments ± standard deviation. The morphology of the empty nanosystems and the PTX-loaded zein nanoparticles was evaluated by means of a Transmission Electron Microscope (CM12 TEM, PHILIPS, The Netherlands) equipped with an OLYMPUS Megaview G2 camera[47]. The amount of PTX retained by the colloidal systems was evaluated through HPLC analysis as previously reported[13]. The entrapment efficiency (EE%) was calculated as the percentage of the total amount of drug that became entrapped, according to the Eq. (1) below:

$$\mathrm{EE\%} = \mathrm{De/Da} \times 100 \tag{1}$$

where De is the quantity of entrapped drug and Da is the quantity of PTX added during the preparation of the systems. The percentage of the ratio between the total weight of the nanoparticles and the amount of drug entrapped was used to express the loading capacity (LC%)[48]. The leakage of the PTX from the zein nanoparticles was evaluated at various pHs (5 and 7.4) using the dialysis method as previously described[15]. In particular, 1 ml of each formulation was placed in a dialysis bag (Spectra/Por with molecular cutoff 12,000–14,000 by Spectrum Laboratories Inc.), secured with clips at both ends, and transferred to a beaker containing 200 ml of a continuously-stirred PBS solution under sink conditions. 1 ml of release medium was removed and replaced with the same volume of fresh solution at different incubation times. The previously mentioned HPLC method was then used to analyze the collected samples. The amount of released PTX was expressed using the following Eq. (2):

$$\mathrm{Release}\,(\%) = \mathrm{drug_{rel}/drug_{load}} \times 100 \tag{2}$$

where $\mathrm{drug_{rel}}$ is the leakage of PTX at the time t and $\mathrm{drug_{load}}$ is the amount of PTX contained within the zein nanosystems.

Surface hydrophobicity and FT-IR analysis

The Rose bengal (RB) assay was used to examine the surface hydrophobicity of the nanosystems[21,47]. In summary, 1 ml of an aqueous solution of RB (0.1 mg/ml) was incubated with various concentrations of nanoparticles (6.33–1.616 mg/ml) for 30 min while being constantly shaken. The samples were then centrifuged for 30 min (4 °C, 90 k × g in an Optima TL Beckman Ultracentrifuge s.r.l., Milan, Italy). The supernatant was collected at the end of the process and examined at 548 nm using a Varioskan Lux microplate reader (Thermo Fischer Scientific, Waltham, Massachusetts, USA). The Total Surface Area (TSA) of the Nanozein was calculated assuming that the carriers were spherical in shape by using the following Eq. (3):

$$\mathrm{TSA} = (\mathrm{SA_{NP}}) \times (\mathrm{NT_{NP}}) \tag{3}$$

where $\mathrm{SA_{NP}}$ corresponds to the surface area of a single nanoparticle ($4\pi r^2$), and $\mathrm{NT_{NP}}$ is the total number of nanoparticles present in the dilution, calculated as the ratio between the weight of the particles in each dilution (mNP) and the density of the zein (ρ, calculated by picnometry as 1.43 g/mL), multiplied for the volume of a single nanoparticle (VNP, $4/3\pi r^3$). The ratio of bound to unbound molecules, or the partitioning quotient of Rose bengal (PQ), was plotted against the TSA of the particles. The acquired slope values indicate the hydrophobicity

of the investigated nanoformulations. A NicoletTM iS5 spectrometer with an iD7 Attenuated Total Reflectance accessory (Thermo Fisher Scientific Inc., Waltham, MA, USA) was used to assess the vibrational spectra of the zein, the SD, the physical mixture, and the freeze-dried Nanozein or NanoPTX. The FT-IR spectra were obtained using 64 acquisitions at a resolution of 4 cm^{-1} and a wave number range of 500–4000 cm^{-1}. The spectral analyses were generated using OMNIC software.

Cell lines and cell culture

The HEY (derived from a moderately differentiated papillary cystadenocarcinoma of the ovary)[49] and the COV362 (derived from human ovarian epithelial-endometroid carcinoma)[50] human cell lines were cultured in DMEM. The cells were all purchased from the American Type Culture Collection (ATCC, Manassas, VA, USA). All media were supplemented with 10% foetal bovine serum, 50U of penicillin and 50 µg of streptomycin/ml (Thermo Fisher Scientific, Milan, Italy). All cell lines were maintained at 37 °C in 5% CO_2.

Reagents/treatments

For all the experiments, the cells were plated in 6-well plates at a density of 5×10^5 cells/well in complete medium. The next day, the cells were treated with different amounts of Nanozein, NanoPTX or PTX for 24 h, and then analysed by flow cytometry. Free PTX (Paclitaxel TEVA, Milan, Italy) was used, at the same final concentration as NanoPTX.

For the cell-uptake experiments, 2×10^5 cells were plated in a 6-well plate in complete medium. After 24 h, HEY and COV362 cells were treated with 5 or 10 µg/ml of fluorescent nanoparticles for 4 h, respectively, washed twice with PBS1 × and the micrographs acquired at 20 × magnification with a Leica LAS X Thunder Imaging System (Leica Microsystems Srl, Milan, Italy).

Cell viability

The hHGS-OC cells were treated with various concentrations of Nanozein (0, 5, 10, 20 and 40 µg/ml) and a propidium iodide (PI) assay was performed after 24 h. Untreated cells were used as a control. In detail, they were centrifuged and the relative pellets were stained with PI. Acquisition of 2.0×10^4 events was carried out with a FACS BD LSR FortessaTM X-20 cytofluorometer (BD Biosciences, Milan, Italy) and the PE-positive fluorescence was analysed with the FlowJo software program (Tree Star, Inc., Ashland, OR, United States)[51,52]. All the experiments were performed in triplicate.

In vitro cytotoxicity assay

The cytotoxicity of the various formulations was evaluated using the MTT assay as a function of the incubation time (24, 48 and 72 h) and drug concentration (0, 3, 6 and 9 nM). Untreated cells were used as a control while empty nanoparticles (tested at the same concentration as the colloidal formulation containing PTX) as a blank. 1.7×10^4 cells/well were plated eightfold in 96-well plates in complete medium and then treated with the various formulations after 24 h.

To assess cell viability, 20 µL of tetrazolium salt (5 mg/mL) solubilized in phosphate-buffered solution was added to each well. The plates were then incubated for an additional 3 h and then the absorbance was measured using a microplate spectrophotometer (Thermo Scientific™Varioskan™ LUX) at a wavelength of 540 nm, with a reference wavelength of 690 nm to account for background absorption. Cell viability was expressed as a percentage and reported as the mean of five independent experiments ± standard deviation and was calculated using the following equation:

$$\text{Cell viability}\ (\%) = \text{AbsT}/\text{AbsC} \times 100$$

where:
AbsT is the absorbance of treated cells.
AbsC is the absorbance of control (untreated) cells.

Evaluation of intracellular ROS

In order to determine the intracellular ROS levels, the incubation of hHGS-OC cells treated with Nanozein (0, 5, 10, 20 and 40 µg/ml) was carried out for 10 min at 37 °C with the redox-sensitive probe 2′-7′-Dichlorodihydrofluoresceindiacetate (CM-H_2DCFDA; Thermo Fisher Scientific, Waltham, USA) according to the instructions of the manufacturer. Untreated cells were used as a control. CM-H_2DCFDA fluorescence was analysed by flow cytometry using a FACS BD LSR Fortessa TM X-20 cytofluorometer (BD Biosciences) and data were processed using FlowJo software (Tree Star, Inc.)[29]. All the experiments were performed in triplicate.

Apoptosis assay

Apoptosis analysis was performed through the Alexa Fluor®488 Annexin V/Dead Cell Apoptosis Kit (Thermo Fisher Scientific, Waltham, Massachusetts, USA). hHGS-OC cells were double stained with Alexa Fluor®488 Annexin V and PI for 15 min at RT in the dark. Each tube was diluted with 400 µl of Annexin Binding Buffer and then analysed by flow cytometry using a FACS BD LSRFortessaTM X-20 cytofluorometer (BD Biosciences)[52]. All data were processed with FlowJo software (Tree Star, Inc.). All the experiments were performed in triplicate.

Statistical analysis

The student's t-test assuming unequal variances between two samples was used to determine significant differences ($p < 0.05$ *, $p < 0.01$ **, $p < 0.001$ ***)[53,54].

Data availability

The raw data supporting the conclusions of this article will be made available by the authors on request.

Received: 1 November 2024; Accepted: 17 February 2025
Published online: 27 March 2025

References

1. Mustafa, G. et al. Nanoscale drug delivery systems for cancer therapy using paclitaxel—A review of challenges and latest progressions. *J. Drug Deliv. Sci. Technol.* **84**, 104494 (2023).
2. Voci, S., Gagliardi, A., Molinaro, R., Fresta, M. & Cosco, D. Recent advances of taxol-loaded biocompatible nanocarriers embedded in natural polymer-based hydrogels. *Gels* **7**, 33 (2021).
3. Gupta, U. et al. Enhanced apoptotic and antican cer potential of paclitaxel loaded biodegradable nanoparticles based on chitosan. *Int. J. Biol. Macromol.* **98**, 810–819 (2017).
4. Chen, Q., Xu, S., Liu, S., Wang, Y. & Liu, G. Emerging nanomedicines of paclitaxel for cancer treatment. *J. Control. Release* **342**, 280–294 (2022).
5. Raza, F. et al. Recent advances in the targeted delivery of paclitaxel nanomedicine for cancer therapy. *Mater. Adv.* **3**, 2268–2290 (2022).
6. Khalifa, A. M., Elsheikh, M. A., Khalifa, A. M. & Elnaggar, Y. S. R. Current strategies for different paclitaxel-loaded Nano-delivery systems towards therapeutic applications for ovarian carcinoma: A review article. *J. Control. Release* **311**, 125–137 (2019).
7. Celano, M. et al. Co-encapsulation of paclitaxel and JQ1 in Zein nanoparticles as potential innovative nanomedicine. *Micromachines* **13**, 1580 (2022).
8. Xiao, K. et al. A self-assembling nanoparticle for paclitaxel delivery in ovarian cancer. *Biomaterials* **30**, 6006–6016 (2009).
9. Bernabeu, E., Cagel, M., Lagomarsino, E., Moretton, M. & Chiappetta, D. A. Paclitaxel: What has been done and the challenges remain ahead. *Int. J. Pharmaceut.* **526**, 474–495. https://doi.org/10.1016/j.ijpharm.2017.05.016 (2017).
10. Desai, N. Challenges in development of nanoparticle-based therapeutics. *AAPS J.* **14**, 282–295 (2012).
11. Adick, A. et al. Challenges of nanoparticle albumin bound (nab™) technology: Comparative study of Abraxane® with a newly developed albumin-stabilized itraconazole nanosuspension. *Eur. J. Pharm. Biopharm.* **193**, 129–143 (2023).
12. Hathout, L. et al. A multi-institutional analysis of adjuvant chemotherapy and radiation sequence in women with stage IIIC endometrial cancer. *Int. J. Radiat. Oncol. Biol. Phys.* **110**, 1423–1431 (2021).
13. Soe, Z. C. et al. Development of Folate-functionalized PEGylated Zein nanoparticles for ligand-directed delivery of paclitaxel. *Pharmaceutics* **11**, 562 (2019).
14. Tivano, F. & Chiono, V. Zein as a renewable material for the preparation of green nanoparticles for drug delivery. *Front. Biomater. Sci.* **2**, 1156403 (2023).
15. Gagliardi, A. et al. Paclitaxel-loaded sodium deoxycholate-stabilized zein nanoparticles: characterization and in vitro cytotoxicity. *Heliyon* **5**, e02422 (2019).
16. Kostov, S. et al. Hereditary gynecologic cancer syndromes–a narrative review. *Onco. Targets. Ther.* **15**, 381–405 (2022).
17. González-Martín, A. et al. Newly diagnosed and relapsed epithelial ovarian cancer: ESMO Clinical Practice Guideline for diagnosis, treatment and follow-up☆. *Ann. Oncol.* **34**, 833–848 (2023).
18. Chung, W.-M. et al. Increase paclitaxel sensitivity to better suppress serous epithelial ovarian cancer via ablating androgen receptor/aryl hydrocarbon receptor-ABCG2 axis. *Cancers (Basel)* **11**, 463 (2019).
19. McMullen, M., Karakasis, K., Rottapel, R. & Oza, A. M. Advances in ovarian cancer, from biology to treatment. *Nat. Cancer* **2**, 6–8 (2021).
20. Srivastav, A. K., Rajput, P. K., Jaiswal, J., Yadav, U. C. S. & Kumar, U. In vitro and in silico investigation of glycyrrhizic acid encapsulated zein nanoparticles: a synergistic targeted drug delivery approach for breast cancer. *Int. J. Biol. Macromol.* **266**, 131368 (2024).
21. Reboredo, C., González-Navarro, C. J., Martínez-Oharriz, C., Martínez-López, A. L. & Irache, J. M. Preparation and evaluation of PEG-coated zein nanoparticles for oral drug delivery purposes. *Int. J. Pharm.* **597**, 120287 (2021).
22. Li, S. et al. Preparation and characterization of a novel conformed bipolymer paclitaxel-nanoparticle using tea polysaccharides and zein. *Carbohydr. Polym.* **146**, 52–57 (2016).
23. Duan, H. et al. A novel electrospun nanofiber system with PEGylated paclitaxel nanocrystals enhancing the transmucus permeability and in situ retention for an efficient cervicovaginal cancer therapy. *Int. J. Pharm.* **650**, 123660 (2024).
24. Kumar, M. et al. Lipid-coated nanocrystals of paclitaxel as dry powder for inhalation: Characterization, in-vitro performance, and pharmacokinetic assessment. *Colloids Surfaces B Biointerfaces* **237**, 113865 (2024).
25. Sakhi, M. et al. Design and characterization of paclitaxel-loaded polymeric nanoparticles decorated with trastuzumab for the effective treatment of breast cancer. *Front. Pharmacol.* **13**, 855294 (2022).
26. Sun, S., Liang, N. A., Kawashima, Y., Xia, D. & Cui, F. Hydrophobic ion pairing of an insulin-sodium deoxycholate complex for oral delivery of insulin. *Int. J. Nanomed.* **6**, 3049–3056 (2011).
27. Pavlič, R., Gjorgoska, M. & Rižner, T. L. Model cell lines and tissues of different HGSOC subtypes differ in local estrogen biosynthesis. *Cancers (Basel)* **14**, 2583 (2022).
28. Scicchitano, S. et al. Enhanced ZNF521 expression induces an aggressive phenotype in human ovarian carcinoma cell lines. *PLoS ONE* **17**, e0274785 (2022).
29. Scicchitano, S. et al. The double-edged sword of oleuropein in ovarian cancer cells: From antioxidant functions to cytotoxic effects. *Int. J. Mol. Sci.* **24**, 842 (2023).
30. Kampan, N. C., Madondo, M. T., McNally, O. M., Quinn, M. & Plebanski, M. Paclitaxel and its evolving role in the management of ovarian cancer. *Biomed. Res. Int.* **2015**, 413076 (2015).
31. Giannakakou, P., Robey, R., Fojo, T. & Blagosklonny, M. V. Low concentrations of paclitaxel induce cell type-dependent p53, p21 and G1/G2 arrest instead of mitotic arrest: Molecular determinants of paclitaxel-induced cytotoxicity. *Oncogene* **20**, 3806–3813 (2001).
32. Wang, F. et al. Taxol inhibits melanoma metastases through apoptosis induction, angiogenesis inhibition, and restoration of E-cadherin and nm23 expression. *J. Pharmacol. Sci.* **93**, 197–203 (2003).
33. Wang, J., Sui, M. & Fan, W. Nanoparticles for tumor targeted therapies and their pharmacokinetics. *Curr. Drug Metab.* **11**, 129–141 (2010).
34. Yao, Y. et al. Nanoparticle-based drug delivery in cancer therapy and its role in overcoming drug resistance. *Front. Mol. Biosci.* **7**, 193 (2020).
35. Blanco, E., Shen, H. & Ferrari, M. Principles of nanoparticle design for overcoming biological barriers to drug delivery. *Nat. Biotechnol.* **33**, 941–951 (2015).
36. Jurj, A. et al. The new era of nanotechnology, an alternative to change cancer treatment. *Drug Des. Devel. Ther.* **11**, 2871–2890 (2017).
37. Liu, G., An, D., Li, J. & Deng, S. Zein-based nanoparticles: Preparation, characterization, and pharmaceutical application. *Front. Pharmacol.* **14**, 1120251 (2023).

38. Parris, N., Cooke, P. H. & Hicks, K. B. Encapsulation of essential oils in zein nanospherical particles. *J. Agric. Food Chem.* **53**, 4788–4792 (2005).
39. Mehta, S. K., Kaur, G. & Verma, A. Fabrication of plant protein microspheres for encapsulation, stabilization and in vitro release of multiple anti-tuberculosis drugs. *Colloids Surfaces A Physicochem. Eng. Asp.* **375**, 219–230 (2011).
40. Karthikeyan, K., Vijayalakshmi, E. & Korrapati, P. S. Selective interactions of zein microspheres with different class of drugs: An in vitro and in silico analysis. *AAPS PharmSciTech* **15**, 1172–1180 (2014).
41. Huang, X. et al. Resveratrol encapsulation in core-shell biopolymer nanoparticles: Impact on antioxidant and anticancer activities. *Food Hydrocoll.* **64**, 157–165 (2017).
42. Hong, S. S. et al. Role of zein incorporation on hydrophobic drug-loading capacity and colloidal stability of phospholipid nanoparticles. *Colloids Surfaces B Biointerfaces* **171**, 514–521. https://doi.org/10.1016/j.colsurfb.2018.07.068 (2018).
43. da Rosa, C. G. et al. Characterization and evaluation of physicochemical and antimicrobial properties of zein nanoparticles loaded with phenolics monoterpenes. *Colloids Surfaces A Physicochem. Eng. Asp.* **481**, 337–344 (2015).
44. Chen, H., Zhang, Y. & Zhong, Q. Physical and antimicrobial properties of spray-dried zein–casein nanocapsules with co-encapsulated eugenol and thymol. *J. Food Eng.* **144**, 93–102 (2015).
45. De Oliveira, J. L. et al. Association of zein nanoparticles with botanical compounds for effective pest control systems. *Pest Manag. Sci.* **75**, 1855–1865 (2019).
46. Huang, R. et al. Dual role of reactive oxygen species and their application in cancer therapy. *J. Cancer* **12**, 5543 (2021).
47. Gagliardi, A. et al. DIFUCOSIN: DIclofenac sodium salt loaded FUCOidan-SericIN nanoparticles for the management of chronic inflammatory diseases. *Int. J. Pharm.* **655**, 124034 (2024).
48. Selvam, S. & Sarkar, I. Bile salt induced solubilization of methylene blue: Study on methylene blue fluorescence properties and molecular mechanics calculation. *J. Pharm. Anal.* **7**, 71–75 (2017).
49. Buick, R. N., Pullano, R. & Trent, J. M. Comparative properties of five human ovarian adenocarcinoma cell lines. *Cancer Res.* **45**, 3668–3676 (1985).
50. van den Berg-Bakker, C. A. M. et al. Establishment and characterization of 7 ovarian carcinoma cell lines and one granulosa tumor cell line: growth features and cytogenetics. *Int. J. cancer* **53**, 613–620 (1993).
51. Battaglia, A. M. et al. Iron affects the sphere-forming ability of ovarian cancer cells in non-adherent culture conditions. *Front. Cell Dev. Biol.* **11**, 1272667 (2023).
52. Vecchio, E. et al. IBTK contributes to B-cell lymphomagenesis in Eμ-myc transgenic mice conferring resistance to apoptosis. *Cell Death Dis.* **10**, 320 (2019).
53. Scicchitano, S., Faniello, M. C. & Mesuraca, M. Zinc finger 521 modulates the Nrf2-notch signaling pathway in human ovarian carcinoma. *Int. J. Mol. Sci.* **24**, 14755 (2023).
54. Di Sanzo, M. et al. Ferritin heavy chain binds peroxiredoxin 6 and inhibits cell proliferation and migration. *Int. J. Mol. Sci.* **23**, 12987 (2022).

Acknowledgements

The authors are grateful to Lynn Whitted for her language revision of this article.

Author contributions

S.S., A.G., M.C.F. and D.C. conceived the work; S.S., A.G., N.A., E.V., C.G. and A.M.B. performed the experiments and analysed the results; S.S. and A.G. wrote the original draft, writing—review and editing; F.S.C., M.C.F. and D.C. provided funds, supervised the experimental work, writing—review and editing. All authors discussed the results and approved the final version of the manuscript.

Declarations

Competing interests

The authors declare no competing interests.

Additional information

Supplementary Information The online version contains supplementary material available at https://doi.org/10.1038/s41598-025-90840-4.

Correspondence and requests for materials should be addressed to M.C.F. or D.C.